Available online at www.sciencedirect.com
ScienceDirect
Journal of Power Sources 164 (2007) 538–543
JOURNAL OF POWER SOURCES
www.elsevier.com/locate/jpowsour

Short communication

A highly active Pt catalyst fabricated on 3D porous carbon

Hirotoshi Yamada [a,*], Taiki Hirai [b], Isamu Moriguchi [a], Tetsuichi Kudo [c]

[a] *Faculty of Engineering, Nagasaki University, 1-14, Bunkyo-Machi, Nagasaki 852-8521, Japan*
[b] *Graduate School of Science and Technology, Nagasaki University, 1-14, Bunkyo-Machi, Nagasaki 852-8521, Japan*
[c] *National Institute of Advanced Industrial Science and Technology, Tsukuba Central 2, 1-1-1, Umezono, Tsukuba, Ibaraki 305-8568, Japan*

Received 31 August 2006; received in revised form 26 October 2006; accepted 27 October 2006
Available online 8 December 2006

Abstract

A highly active Pt/carbon catalyst for polymer electrolyte membrane fuel cells and direct methanol fuel cells was prepared by using porous carbon that was synthesized by a colloidal-crystal templating method. The microstructure of the Pt/porous carbon composites was studied with N_2 ad-/desorption isotherms, X-ray diffraction and transmission electron microscopy. In contrast to conventional carbon supports, the porous carbon exhibited an attractive microstructure as a catalyst support, i.e. a large surface area with mono-dispersed three-dimensionally interconnected mesopores (45 nm). A large mesopore surface area prompted dispersion of Pt particles, which resulted in a large effective surface area of Pt with a high activity for the oxygen reduction reaction. The porous structure facilitated smooth mass transportation to give rise to high limiting currents.
© 2006 Elsevier B.V. All rights reserved.

Keywords: PEMFC; DMFC; Porous carbon; Oxygen reduction reaction

1. Introduction

For the last few decades, polymer electrolyte membrane fuel cells (PEMFCs) and direct methanol fuel cells (DMFCs) have attracted great interest as alternative power sources for vehicles and mobile electric equipment due to their low pollutant emission levels and high energy densities. In spite of many efforts and improvements by thousands of scientists, PEMFCs and DMFCs have not been commerically used. One of the most critical problems is the cost of platinum catalysts on the electrodes. Pt fine particles are dispersed on carbon blacks with a large surface area to reduce the total Pt amount and to enhance the catalyst activity. The activity depends not only on the primary structure of the catalyst Pt/carbon composites (i.e. carbon surface area, Pt particle size, Pt surface area, etc.), but also on the secondary structure (i.e. aggregation and agglomeration of carbon grains) [1–3]. Commonly used carbon blacks, e.g. Vulcan XC-72, exhibit microscopic structure of aggregation and agglomeration of carbon grains with a size of 30–70 nm. The agglomeration gives rise to voids or pores, which facilitate transportation of reactants and products. Such porous structures also play an important role when polymer electrolyte layers are fabricated on Pt/carbon surfaces as proton conductive paths from catalysts to electrolyte membranes. The polymer electrolyte layers should be homogeneous, interconnected [1–3] and thin [4] on the Pt/carbon surfaces to achieve high efficiency. The pores of carbons should be so large that the polymer electrolytes can penetrate and deposit on the inner surfaces. Fig. 1 schematically shows one plausible microstructure of a FC electrodes. The inner surface of the pores could be easily coated with polymer electrolytes without aggregation or isolation, and all the Pt surfaces are accessible to the reactants (H_2, O_2 and CH_3OH). In the case of carbon blacks, however, it is difficult to control the porous structure. In this context, porous carbons that are fabricated by using colloidal crystals as templates are attractive and characterized by mono-dispersed 3D interconnected mesopores (larger than 2 nm and smaller than 50 nm in diameter, according to IUPAC definition) or macropores (larger than 50 nm) and large meso-/macropore surface areas (>500 $m^2\,g^{-1}$, depending on pore sizes). We have so far demonstrated highly electrochemically effective surfaces of the porous carbon for electrochemical double layer capacitors (200–350 $F\,g^{-1}$) [5–7]. We have also reported that such porous electrodes facilitate high rate capability of Li-ion batteries due to smooth ion transportation in pores [8–10]. A few studies have been reported on the Pt/porous-carbon catalysts, which exhibited better performance in contrast

* Corresponding author. Tel.: +81 95 8192861; fax: +81 95 8192861.
E-mail address: h-yama@nagasaki-u.ac.jp (H. Yamada).

0378-7753/$ – see front matter © 2006 Elsevier B.V. All rights reserved.
doi:10.1016/j.jpowsour.2006.10.074

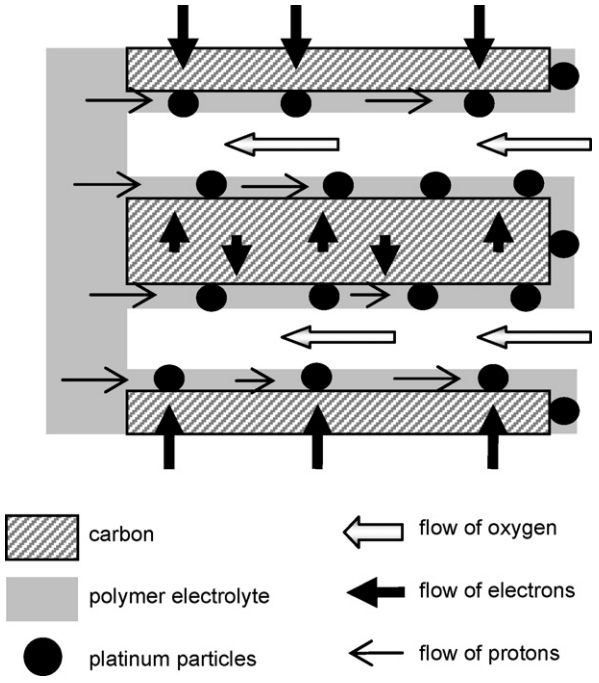

Fig. 1. Schematic drawing of a cathodic electrode of Pt/porous carbon catalyst.

to Pt on non-porous carbons [11,12]. However, in these studies, Pt activity (or Pt surface area) and the aggregation of Pt particles were not investigated and it is difficult to evaluate the effect of the porous structure. In this study, we fabricated Pt/porous carbon catalysts using colloidal crystal templating technique. The microstructures of carbons and Pt particles were investigated in details and their influence on the catalyst activity were reported.

2. Experimental

Porous carbon was synthesized in four steps by using silica colloidal crystals as templates, which has been reported elsewhere [5–7]. Firstly, SiO_2 colloidal crystals were fabricated by centrifuging mono-dispersed colloidal silica particles with an average diameter of 45 nm (SI-45P, Catalysts & Chemicals Ind. Co., Ltd.). Then, phenolic (Novolac) resin was synthesized in the interstitial space among the SiO_2 particles from phenol, formaldehyde and a small amount of concentrated hydrochloric acid. Next, the resin was carbonized at 1000 °C for 5 h in an Ar gas flow. Finally, the SiO_2 templates were removed from the carbon/SiO_2 composites by an aqueous HF solution and the resultant porous carbon were rinsed in de-ionized water and were dried. The porous carbon thus obtained was denoted as C[45].

Platinum fine particles were deposited on carbon surfaces by reducing H_2PtCl_6 as follows. C[45] was dispersed in a tetrahydrofuran solution of H_2PtCl_6 by an ultrasonic treatment. The weight ratio of Pt to C in the starting materials was 0.13:0.87. After formic acid was added as a reducing agent, the solution was refluxed for 6 h. Then the dispersing carbon was collected by filtration and washed with de-ionized water. Finally Pt/porous carbon composite was obtained. Hereafter, the Pt/porous carbon composite is denoted as C[45]:Pt13. Loading of Pt in the composite was estimated from the weight loss in a thermal gravimetry (TG) on a TG/DTA6200 (Seiko Instruments Inc.) in air flow. Microstructures of Pt/carbon composites were observed by transmission electron microscopy (TEM) on a JEOL JEM-2010. Pore parameters were obtained by the analysis of nitrogen adsorption–desorption isotherms recorded at 77 K on a Gemini2375 (Micrometrics Co.). Total specific surface area (S_{total}) was determined by analyzing α_s-plot based on the subtracting pore effect (SPE) method [13,14]. Specific surface area of mesopores and outermost surface (S_{meso}) was analyzed by using *t*-plots [15]. Specific surface area of micropores (S_{micro}; pore size < 2 nm) was estimated by subtracting S_{meso} from S_{total}. X-ray diffraction patterns were recorded on a RINT-2200 (Rigaku Corp., with Ni-filtered Cu Kα) to investigate crystal structures of carbon and platinum. For reference, Pt/carbon composites were prepared in the same way using Vulcan XC-72 (denoted as VC, supplied by Cabot Corp.), acetylene black (AB, Denki Kagaku Kogyo) and activated carbon (AC, Wako Pure Chemical Industries Ltd.).

The catalyst activity of carbon-supported Pt was electrochemically investigated in a 1 M H_2SO_4 aqueous solution at 25 °C. Pt/carbon composites, mixed with 5 wt% poly(tetrafluoroethylene), were pressed onto gold mesh to be served as working electrodes. The geometrical size of the electrodes was ca. 1 cm × 1 cm. A Ag/AgCl/sat'd KCl electrode and a platinum wire were used as reference and counter electrodes, respectively. All the potentials in this paper are referenced to Ag/AgCl/sat'd KCl. The electrochemically active surface areas of Pt particles were studied by cyclic voltammetry using under potential deposition of proton on an electrochemical interface S1287 (Solartron Analytical Inc.), after dissolving oxygen was eliminated from the electrolyte by N_2 bubbling for 30 min. The oxygen reduction activity was measured by potentio-statically in the electrolyte solution, while oxygen was bubbled into the solution under stirring at a constant rate.

3. Results and discussion

3.1. Preparation of Pt/carbon composites

TG confirmed that Pt/carbon ratio of the composites agreed well with that expected from the amount of the starting materials, which indicates that all Pt was successfully loaded on carbon surfaces. Fig. 2 shows the specific surface area of the Pt/C[45] composites as a function of Pt loading. Note that the specific surface areas are based on the weight not of the composites but of the carbons. Obviously, with increasing Pt-loading, S_{meso} exhibited an increasing trend, while S_{micro} decreased. To understand the change of surface areas, it is helpful to know the porous structure of C[45]: the mesopores of C[45] are derived from template SiO_2 particles, whereas the micropores are formed on carbonization of phenolic resin [5–7]. Accordingly, micropores exist in mesopore walls. With this fact, the surface areas of Pt/C[45] composites suggests that Pt particles covered the micropore entrances of mesopores. One may suppose that Pt particles were deposited inside the micropores, but this is denied by the

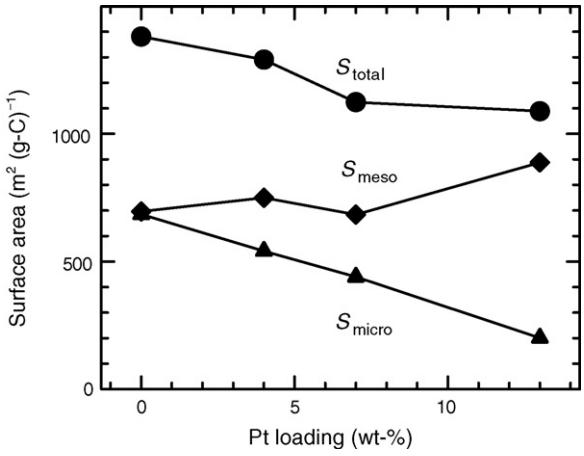

Fig. 2. Specific surface area of Pt/C[45] composites based on the carbon weight.

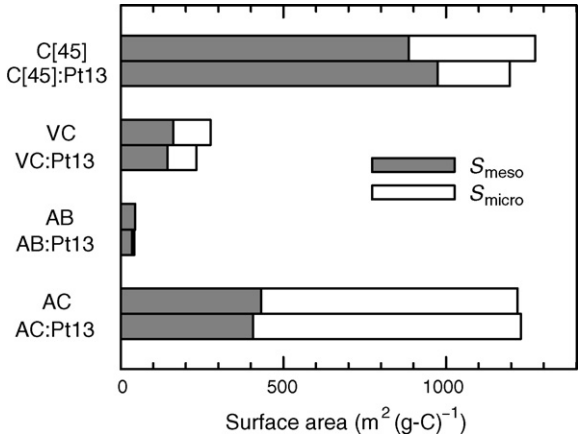

Fig. 3. Comparison of surface area of carbons and Pt/carbon composites.

fact that S_{meso} did not decrease with the increase in Pt loading. Fig. 3 compares the specific surface areas of the carbons and the Pt/carbon composites used in this study. Obviously, C[45] and C[45]:Pt13 exhibited very large S_{meso} more than 500 m^2 g^{-1}. For VC, AB and AC, S_{meso} decreased by Pt-loading, which suggests aggregation of Pt particles.

X-ray diffraction patterns of the Pt/carbon composites are shown in Fig. 4. Profiles revealed the deposition of Pt for all the carbon supports. The crystalline sizes of Pt, estimated from the peak width of (1 1 1) diffraction using Scherrer's equation, are listed in Table 1. C[45]:Pt13 exhibited the smallest crystalline size of 5 nm. Although large crystalline sizes were obtained for VC:Pt13 and AB:Pt13, broad peak bottoms of these two composites imply distribution of the crystalline sizes, i.e. the diffraction

Table 1
Sizes of Pt particles on carbon supports, obtained from XRD and TEM

Composites	Crystalline size (XRD) (nm)	Particle size (TEM) (nm)
C[45]:Pt13	5	5 ± 2
VC:Pt13	15	6 ± 2
AB:Pt13	18	8 ± 3
AC:Pt13	12	10 ± 5

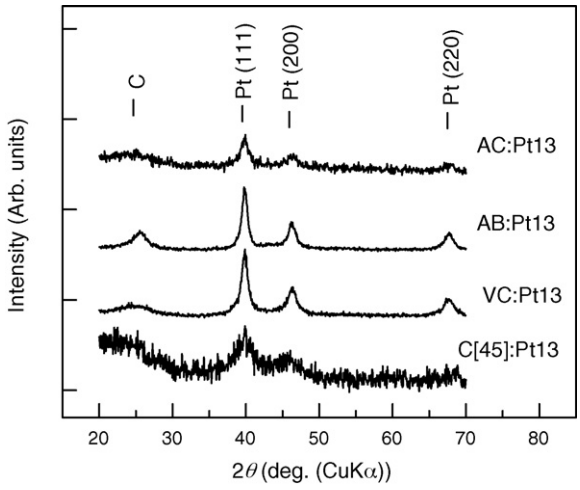

Fig. 4. XRD profiles of Pt/carbon composites.

from large crystallines were so strong and outstanding that the weak diffraction from small crystallines was hidden.

Fig. 5a–d displays TEM images of the Pt/carbon composites. For C[45]:Pt13, C[45] exhibited three dimensionally interconnected spherical mesopores with a diameter of 45 nm (Fig. 5a), which agrees the template SiO_2 particle size. On the inner surface of the mesopores, small Pt particles were homogeneously scattered. The TEM observation supports the suggestion from the change of specific surface area of Pt/C[45] composites that the decrease in S_{micro} of C[45] is due to the coverage of micropore mouths in mesopore walls with Pt particles. For VC and AB, it was found that small carbon grains (20–50 nm) form grape-like aggregations and VC exhibits agglomeration with void (ca. 100 nm in diameter). For VC, Pt particles were found to be dispersed on the carbon surface but aggregation of Pt particles was also observed. For AB, Pt particles were rather aggregated. This aggregation is possibly caused by the small surface area of VC and AB (see Fig. 3). For AC, carbon grains with diameters of 10–30 nm aggregated and agglomerated. Pores among the agglomerated carbon grains were 50–100 nm in size. In contrast to VC and AB, AC seems rather desirable to load Pt particles with the porous structure as well as the larger surface area (Fig. 2), but, in reality, heavily aggregated Pt particles were found on the AC surfaces. The heavy aggregation on the AC is probably related to the functional groups covering the surface (e.g., C–OH, C=O, COOH and etc.), which were generated on the activation reactions with H_2O vapor or CO_2 at high temperatures. These functional groups would exhibit affinity for the Pt precursor and some of them may directly reduce the precursor. As a result, Pt is deposited rapidly on a certain parts of AC surfaces before the precursor can diffuse to all surfaces.

The Pt particle sizes observed in the TEM images are listed in Table 1. For C[45]:Pt13 and AC:Pt13, particle sizes from the TEM images agreed well with the crystalline size, while for VC:Pt13 and AB:Pt13, a few particles were as large as the crystalline sizes estimated from XRD patterns, but many smaller particles were also observed This particle size distribution gave rise to the broad peak bottoms of XRD profiles of VC:Pt13 and AB:Pt13.

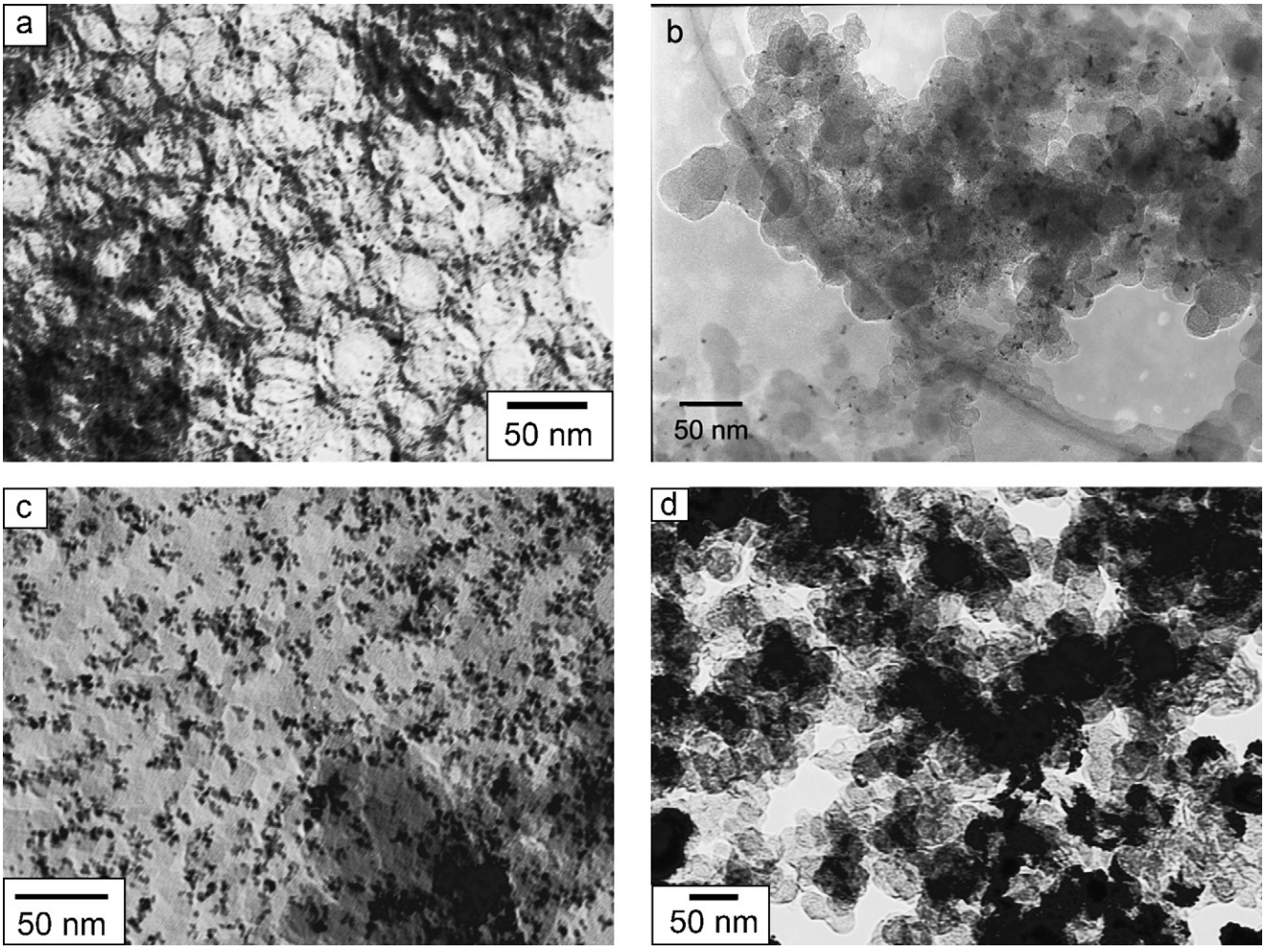

Fig. 5. TEM images of Pt/carbon composites. (a) C[45]:Pt13, (b) VC:Pt13, (c) AB:Pt13 and (d) AC:Pt13.

3.2. Electrochemical catalyst activities

Fig. 6 demonstrates a cyclic voltammogram (10 mV s^{-1}) of C[45]:Pt13 in 1 M H_2SO_4 where dissolved O_2 was eliminated. In the anodic process, a peak related to desorption of hydrogen atoms from the Pt surface was observed around −0.2 to 0 V. The charge due to hydrogen desorption was estimated by subtracting the background current caused by charging the double layer capacitance of the porous carbon. A minimum current around 0.1–0.2 V was used as the background current. By using the specific capacity of 210 μC (cm Pt)$^{-2}$ for the under-potential deposition of protons on Pt, the effective Pt surface area and average Pt particle diameters were estimated, which are listed in Table 2. The Pt diameter of C[45]:Pt13 agreed well with those obtained from XRD and TEM, while that of AB:Pt13 and AC:Pt13 were larger than values in Table 1. These results confirm the homogeneous dispersion of Pt particles for C[45]:Pt13 and the aggregation for AB:Pt13 and AC:Pt13, as mentioned in Section 3.1.

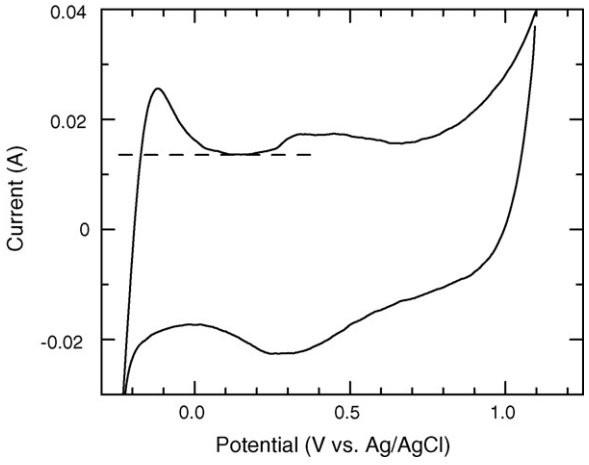

Fig. 6. Cyclic voltammogram of C[45]:Pt13 in 1 M H_2SO_4 with a sweep rate of 10 mV s^{-1}. A dashed line indicates a baseline of hydrogen desorption from Pt surfaces.

Table 2
Effective surface area and diameter of Pt particles of Pt/carbon composites

Composites	Pt surface area (cm^2 (g Pt)$^{-1}$)	Pt diameter (nm)
C[45]:Pt13	686	5.0
VC:Pt13	233	15
AB:Pt13	150	23
AC:Pt13	76	46

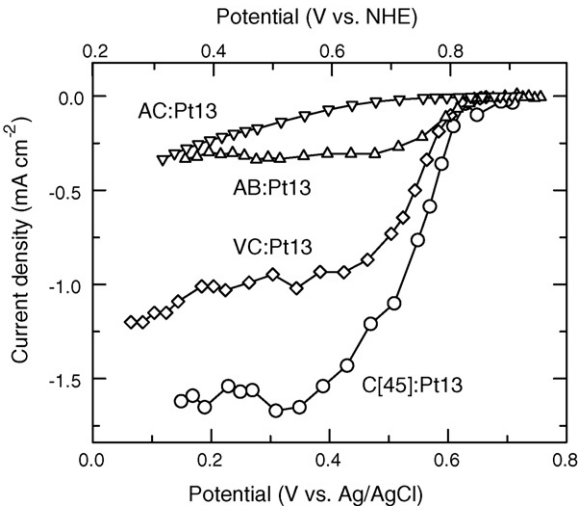

Fig. 7. Current–potential curves of oxygen reduction in 1 M H_2SO_4 of Pt/carbon composites.

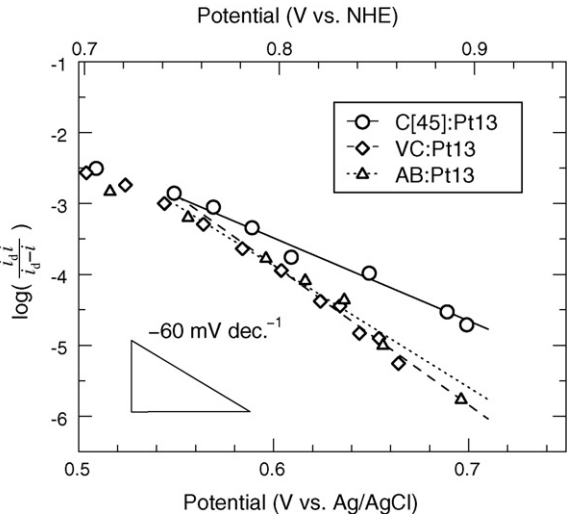

Fig. 8. Tafel plots for the oxygen reduction with the Pt/carbon composites. Current density was corrected for mass-transfer effect.

Fig. 7 exhibits current–potential curves of oxygen reduction on the Pt/carbon composites, where current density is based on the electrode areas. For C[45]:Pt13, VC:Pt13 and AB:Pt13, with decreasing potential, the cathodic current density increased and leveled off due to limitation in the mass transportation of oxygen. On the other hand, AC:Pt13 did not exhibit saturation of current, because the activity of the AC:Pt13 was too low. Among the former three composites, the limiting current density decreased in the order of C[45]:Pt13 > VC:Pt13 > AB:Pt13. The carbon dependence indicates that the rate determining process is not the oxygen diffusion through the diffusion layer at the interfaces of the electrode and the bulk electrolyte solution. The current density was limited by the oxygen transportation through the electrodes, i.e., in pores or among carbon grains (represented by white arrows in Fig. 1). The largest limiting current density of C[45]:Pt13 is accounted for by the smooth electrolyte transportation in pores. And the more porous structure of VC:Pt13 caused higher limiting current than for AB:Pt13.

Pt activity on oxygen reduction of Pt/carbon composites is compared by Tafel plot in Fig. 8 and Table 3. Note that the current density is corrected for mass-transport effects by calculating $i_d i/(i_d - i)$, where i_d and i are diffusion-limiting current density and observed current density, respectively. All the plots showed straight region with a slope of −55 to −83 mV decade^{-1} around 0.6–0.7 V, which corresponds to ca. 0.8–0.9 V versus standard hydrogen electrode [16]. It has been explained that O_2 reduction occurring on Pt-oxide covered surface in this potential range [17]. In contrast to the typical reported value of −60 mV decade^{-1} [18–21], the slope of C[45]:Pt13 (−85 mV decade^{-1}) was slightly higher, which may result from a different mechanism of the oxygen reduction reaction. As listed in Table 3, C[45]:Pt13 exhibited the highest activity, which are explained by the largest Pt surface area and may also be caused by the different reaction mechanism suggested above.

The high catalyst activity and high limiting current density of Pt/porous carbon are effective not only in oxygen reduction but also in methanol oxidation for DMFCs. The porous structure would be also advantageous for coating polymer electrolyte layers, which will be demonstrated in a further study.

Table 3
Mass-transfer-corrected current density on oxygen reduction current in Tafel region of Pt/carbon composites

Composites	Mass-transfer-corrected current density[a] at 0.6 V (A cm^{-2})
C[45]:Pt13	3.4×10^{-4}
VC:Pt13	1.4×10^{-4}
AB:Pt13	1.4×10^{-4}

[a] Current density is based on electrode surface area.

4. Conclusions

In this paper, a Pt/carbon catalyst for PEMFCs and DMFCs was prepared by using three dimensionally interconnected porous carbons as supports. In contrast to Vulcan XC-72, acetylene black and activated carbon, platinum particles on the porous carbon exhibited a large mesopore surface area that facilitated dispersion of small Pt particles (ca. 5 nm). The porous structure promoted smooth electrolyte transportation, which resulted in a high limiting current density. The well-scattered platinum particles exhibited a very high activity, which may allow reduction of the Pt amounts used for FC catalysts.

Acknowledgements

Thanks are due to Mr. Hiroshi Furukawa for his technical supports and TEM operation.

References

[1] M. Uchida, Y. Aoyama, N. Eda, A. Ohta, J. Electrochem. Soc. 142 (1995) 4143.
[2] M. Uchida, Y. Fukuoka, Y. Sugawara, N. Eda, A. Ohta, J. Electrochem. Soc. 143 (1995) 2245.

[3] M. Uchida, Y. Fukuoa, Y. Sugawara, H. Ohara, A. Ohta, J. Electrochem. Soc. 145 (1998) 3708.
[4] E. Higuchi, H. Uchida, M. Watanabe, J. Electroanal. Chem. 583 (2005) 69.
[5] I. Moriguchi, F. Nakahara, H. Furukawa, H. Yamada, T. Kudo, Electrochem. Solid-State Lett. 7 (2004) A221.
[6] I. Moriguchi, F. Nakahara, H. Yamada, T. Kudo, Studies Surf. Sci. Calal. 156 (2005) 589.
[7] H. Yamada, H. Nakamura, F. Nakahara, I. Moriguchi, T. Kudo, J. Phys. Chem. C, in press.
[8] I. Moriguchi, R. Hidaka, H. Yamada, T. Kudo, H. Murakami, N. Nakashima, Adv. Mater. 18 (2006) 69.
[9] H. Yamada, T. Yamato, I. Moriguchi, T. Kudo, Chem. Lett. 33 (2004) 1548.
[10] H. Yamada, T. Yamato, I. Moriguchi, T. Kudo, Solid State Ionics 175 (2004) 195.
[11] G.S. Chai, I.S. Shin, J.-S. Yu, Adv. Mater. 22 (2004) 2057.
[12] F. Su, X.S. Zhao, Y. Wang, J. Zeng, Z. Zhou, J.Y. Lee, J. Phys. Chem. B 109 (2005) 20200.
[13] K.S.W. Sing, Carbon 27 (1989) 5.
[14] K. Kaneko, C. Ishii, M. Ruike, H. Kuwabara, Carbon 30 (1992) 1075.
[15] B.C. Lippens, J.H. de Boer, J. Catal. 4 (1965) 319.
[16] A.J. Bard, L.R. Faulkner, Electrochemical Methods, Fundamentals and Applications, 2nd ed., John Wiley & Sons Inc., New Jersey, 2000, p. 3.
[17] A. Parthasarathy, C.R. Martin, S. Srinivasan, J. Electrochem. Soc. 138 (1991) 916.
[18] Y. Takasu, N. Ohashi, X.-G. Zhang, Y. Murakami, H. Minagawa, S. Sato, K. Yahikozawa, Electrochim. Acta 41 (1996) 2595.
[19] U.A. Paulus, T.J. Schmidt, H.A. Gasteiger, R.J. Behm, J. Electroanal. Chem. 495 (2001) 134.
[20] T.J. Schmidt, U.A. Paulus, H.A. Gasteiger, R.J. Behm, J. Electroanal. Chem. 508 (2001) 41.
[21] N. Wakabayashi, M. Takeichi, M. Itagaki, H. Uchida, M. Watanabe, J. Electroanal. Chem. 574 (2005) 339.